Cardiovascular Engineering and Technology
https://doi.org/10.1007/s13239-023-00701-2

BMES BIOMEDICAL ENGINEERING SOCIETY

ORIGINAL ARTICLE

# Virtual Planning and Patient-Specific Graft Design for Aortic Repairs

**Seda Aslan[1] · Xiaolong Liu[1,5] · Qiyuan Wu[1] · Paige Mass[2] · Yue-Hin Loke[2] · Jed Johnson[3] · Joey Huddle[3] · Laura Olivieri[2] · Narutoshi Hibino[4] · Axel Krieger[1]**

Received: 19 October 2022 / Accepted: 7 November 2023


## Abstract

**Purpose** Patients presenting with coarctation of the aorta (CoA) may also suffer from co-existing transverse arch hypoplasia (TAH). Depending on the risks associated with the surgery and the severity of TAH, clinicians may decide to repair only CoA, and monitor the TAH to see if it improves as the patient grows. While acutely successful, eventually hemodynamics may become suboptimal if TAH is left untreated. The objective of this work aims to develop a patient-specific surgical planning framework for predicting and assessing postoperative outcomes of simple CoA repair and comprehensive repair of CoA and TAH.

**Methods** The surgical planning framework consisted of virtual clamp placement, stenosis resection, and design and optimization of patient-specific aortic grafts that involved geometrical modeling of the graft and computational fluid dynamics (CFD) simulation for evaluating various surgical plans. Time-dependent CFD simulations were performed using Windkessel boundary conditions at the outlets that were obtained from patient-specific non-invasive pressure and flow data to predict hemodynamics before and after the virtual repairs. We applied the proposed framework to investigate optimal repairs for six patients ($n=6$) diagnosed with both CoA and TAH. Design optimization was performed by creating a combination of a tubular graft and a waterslide patch to reconstruct the aortic arch. The surfaces of the designed graft were parameterized to optimize the shape.

**Results** Peak systolic pressure drop (PSPD) and time-averaged wall shear stress (TAWSS) were used as performance metrics to evaluate surgical outcomes of various graft designs and implantation. The average PSPD improvements were 28% and 44% after the isolated CoA repair and comprehensive repair, respectively. Maximum values of TAWSS were decreased by 60% after CoA repair and further improved by 22% after the comprehensive repair. The oscillatory shear index was calculated and the values were confirmed to be in the normal range after the repairs.

**Conclusion** The results showed that the comprehensive repair outperforms the simple CoA repair and may be more advantageous in the long term in some patients. We demonstrated that the surgical planning and patient-specific flow simulations could potentially affect the selection and outcomes of aorta repairs.

**Keywords** Virtual graft design · Aorta repair · Coarctation · Transverse arch hypoplasia · Surgical planning · Computational fluid dynamics

## Abbreviations

| | |
|---|---|
| CoA | Coarctation of aorta |
| TAH | Transverse arch hypoplasia |
| AAo | Ascending aorta |

Associate Editor Alison Marsden oversaw the review of this article.

✉ Seda Aslan
saslan2@jhu.edu

[1] Department of Mechanical Engineering, Johns Hopkins University, 3400 North Charles Street, Baltimore, MD 21218, USA

[2] Division of Cardiology, Children's National Hospital, Washington, DC, USA

[3] Nanofiber Solutions, Dublin, OH, USA

[4] Section of Cardiac Surgery, Department of Surgery, The University of Chicago Medicine, Chicago, IL, USA

[5] Department of Mechanical Engineering, Texas Tech University, Lubbock, TX, USA

Published online: 20 November 2023

| | |
|---|---|
| DAo | Descending aorta |
| BCA | Brachiocephalic artery |
| LCCA | Left common carotid artery |
| LSA | Left subclavian artery |
| PA | Pulmonary artery |
| EEEA | Extended end-to-end anastomosis |
| MRI | Magnetic resonance imaging |
| BSA | Body surface area |
| WK | Windkessel |
| PSPD | Peak systolic pressure drop |
| TAWSS | Time-averaged wall shear stress |
| OSI | Oscillatory shear index |

## Introduction

Coarctation of aorta (CoA) is one of the most common congenital heart diseases that affect approximately 4 out of 1000 newborns in the US every year [1]. CoA is defined as a narrowing in the descending aorta (DAo) which restricts the blood flow to the lower body. The severe restriction of blood flow in the aorta significantly affects the hemodynamics and results in life-threatening conditions such as upper body hypertension [2], aortic aneurysm formation [3], early onset coronary artery disease [4] etc. The guideline for the treatment of CoA in patients is a peak systolic pressure drop (PSPD) of 20 mmHg or higher [5] that is measured between upper and lower extremities. The common techniques to repair CoA are stent placement in the narrowed region [1], transcatheter balloon angioplasty [6], and extended end-to-end surgical anastomosis. While transcatheter treatments are minimally invasive and offer faster recovery, they can only address isolated CoA. However, CoA may coexist with transverse arch hypoplasia (TAH), which represents a constriction over a more extensive area of the aortic arch, specifically where the vessels to the head and neck begin. Given the multiple branches in the arch region, addressing TAH requires a specific resection path and suture line, making the repair considerably complex.

TAH precludes stent placement and requires surgical repair, which carries a different level of risk. Clinicians base their decisions on patient-specific risks and benefits of each scenario.

In patients who suffer from both CoA and TAH, the common surgical techniques to repair the aorta include extended end-to-end anastomosis (EEEA) and patch repair [7]. EEEA involves resection of the narrowed part in the descending aorta, making an incision on the lower surface of the TAH, and stretching the open end of descending aorta to suture both ends of the native tissue [8] which may result in gothic arch shape [9]. On the other hand, repairing the aorta using pulmonary patch homograft [10] requires an open-heart procedure with support of cardiopulmonary bypass. It is an alternative surgical repair technique that yields better post-operative mid and long-term results compared to EEEA. For the patch repair, the stenotic regions are resected, followed by making an incision on the lower surface of the transverse arch extending to the origin of the innominate artery. A pulmonary artery (PA) homograft, is used to reconstruct the aortic arch [7]. The patch repair technique was demonstrated in Fig. 1c, while Fig. 1a and b showcased the stent placement and EEEA for comparison. Since the creation of the patch and the reconstruction of the aorta are performed with acute time pressure under bypass, post-operative complications are more likely to occur than using other non-invasive repairs. Depending on the severity of TAH and the risks associated with such extensive surgery, surgeons may conservatively repair only CoA in some patients. However, even when the repair of CoA alone reduces PSPD below 20 mmHg in some cases, late complications may still occur due to existing TAH [11]. Prior studies [12], reported that 50% of patients post-CoA repair faced arch reobstruction over an extended period. There is a need to predict and assess various plans of aortic surgical repairs preoperatively.

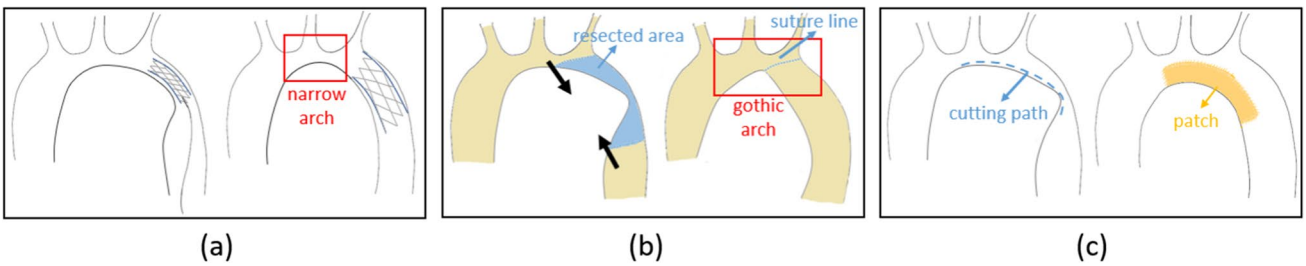


**Fig. 1** Examples of **a** endovascular and **b**, **c** open surgical repairs. **a** displays a stent placement for CoA repair, **b** demonstrates EEEA for CoA and TAH repair. The blue region is resected, and the rest of the tissues are extended and anastomosed together. **c** shows an aorta reconstruction using a patch for CoA and TAH repair. The narrowing in the arch that could remain after stent placement and the gothic arch that may form after EEEA can be prevented using a patch demonstrated in **c**. EEEA extended end-to-end anastomosis, CoA coarctation of aorta, TAH transverse arch hypoplasia

Virtual surgical planning has been used to identify optimal patient-specific options of cardiovascular surgery, such as Fontan operation [13–17] with optimal post-operative outcome prediction. In these studies, three-dimensional (3D) modeling of Fontan grafts is performed using computer-aided design, followed by iterative hemodynamic simulations using pre-operative imaging data and virtually reconstructed vessel structures to predict post-operative outcomes. Different from designing Fontan grafts that are in tubular shapes, virtual planning of aortic arch surgery involves dealing with geometrically complex anatomy with supra-aortic branches and is further complicated by pulsatile blood flow. The state-of-the-art research has been focusing on virtual planning of CoA repairs [18, 19] and has shown potential to improve the surgical outcomes of PSPD and wall shear stress (WSS). However, the surgical planning process is yet to be used to predict and evaluate the outcomes of comprehensive aortic repairs.

The research challenge of virtual surgical planning for patients with both CoA and TAH is threefold. First, virtual plans should realistically mimic the surgery. Virtual dissection should be performed after the isolation of stenotic areas. The underlying problem is how to effectively isolate these areas during virtual surgical planning. Second, given the patient's native aortic vessel geometry and the surgical restrictions, identifying patient-specific vascular grafts for aortic vessel reconstruction with optimized postoperative hemodynamic performance is challenging. The underlying problems are how to efficiently explore and design patient-specific aortic graft geometries that are manufacturable, and how to evaluate performance of different aortic repairs. Third, because TAH repair carries significant risk to the patient, the necessity of performing arch repair or only CoA repair should be carefully evaluated to ensure that the patient's benefit to risk ratio is high enough. Methods to evaluate the benefits of CoA repair with or without TAH repair using virtual surgical planning have yet to be established.

To address these challenges, we developed a patient-specific virtual surgical planning framework for aortic repairs. We performed virtual aortic repairs for six patients (n = 6), who suffer from co-existing CoA and TAH. Our primary contributions include: 1) Creation and placement of virtual clamps that mimic the surgery to isolate the region requiring surgery, 2) Design of a novel graft shape for comprehensive surgical repair of TAH and CoA and manufacture of the graft using a tissue-engineering technique to show the feasibility of generating this novel shape, and 3) Performing flow simulations to systematically compare our virtual comprehensive repairs against virtual isolated CoA repairs. The virtual surgical planning of aortic repairs could help surgeons to comprehensively review the vessel reconstruction outcomes and make better surgical decisions for the patient's long-term health benefits.

## Methods

Figure 2 shows our virtual surgical planning framework for comprehensive aortic repair. The framework starts with 3D reconstruction of aortic anatomy using magnetic resonance imaging (MRI) data (Fig. 2a). Surgical clamps are virtually modeled according to their actual dimensions and were placed in the aorta to separate the regions requiring repair (Fig. 2b). Comprehensive repair was performed to reconstruct the arch and DAo by replacing the stenotic regions with a hemodynamically optimized graft (Fig. 2c-d). Finally, an optimized graft was manufactured using electrospun nanofibers (Fig. 2e).

### Reconstruction of 3-D Native Aorta Anatomy

The images of the native aorta anatomies of six ($n = 6$) patients were acquired from MRI as part of an Institutional Review Board (IRB) approved retrospective study. The MRI data included contrast-enhanced, subtracted magnetic resonance angiography (MRA) and three-phase velocity flow

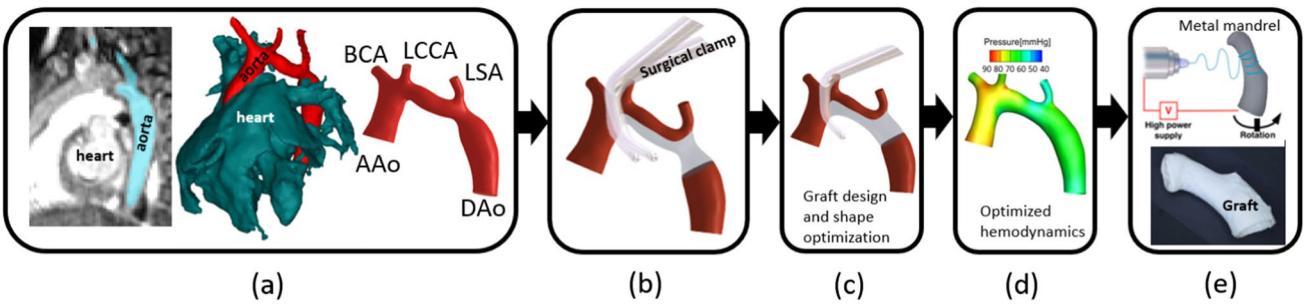


**Fig. 2** Schematic of the surgical planning framework: **a** reconstruction of 3-D native aorta anatomy, **b** virtual clamp placement and virtual resection, **c** design and optimization of patient-specific graft, **d** hemodynamics simulations, and **e** manufacture of the graft

cines in the ascending aorta (AAo) and DAo. The MRA consisted of a non-gated, breath-held acquisition with pixel size 1.4x1.4 mm, which was used to segment a 3D model of the aorta using image segmentation software (Mimics; Materialise, Leuven, Belgium). The 3D anatomy of the aorta included AAo, DAo, and three supra-aortic branches (brachiocephalic artery (BCA), left common carotid artery (LCCA), and left subclavian artery (LSA)), shown in Fig. 2a. The 3-D geometry was then smoothed using Meshmixer software (San Rafael, CA, USA). Using SolidWorks (Waltham, MA, USA), boundary cuts were made perpendicular to the flow direction at the aorta boundaries where the time-dependent flow rates were measured.

## Virtual Clamping of the Aorta

Before performing an extended end-to-end repair of both CoA and TAH, surgeons place a clamp on the aorta to create a temporary bloodless field to address the stenotic region and perform the repair. Although somewhat variable, typical placement of the clamp is in the proximal transverse arch, between the BCA and LCCA. This position allows for access to the entire region requiring repair while maintaining cerebral blood flow through the BCA during the surgery. Although excessive tension on the clamp at this location may obstruct the AAo, the complications can be prevented by monitoring the right radial artery pressure [20].

We simulated the procedure in our TAH repair by placing a virtual clamp between BCA and LCCA (Fig. 3). The sizes of the pediatric aorta clamps (Beck Infant Aorta Clamp - Angled DeBakey Atraumatic jaws, Wexler Surgical) were selected patient-specifically based on the aorta dimensions. Depending on the available space in the heart region, the surgeon may rotate and place the clamp closer to the proximal arch. This operation allows exposing a larger region

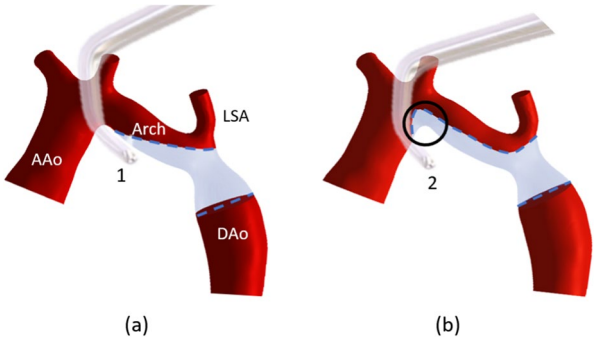


**Fig. 3** Clamp placement and different paths (blue dashed lines) on the aortic arch to perform virtual resection **a** the resection is performed using a straight cut in the arch, **b** clamp is placed in position 2 by rotating the clamp in position 1 clockwise. The resection path is a spline curve in the arch. The region of repair extended to the distal AAo (circled area)

to modify the shape of the aortic arch. Based on this clinical practice, to mimic the surgical clamp placement and to investigate the effects of clamp position on comprehensive aorta repair, we rotated the clamp clockwise resulting in having a larger area in the arch to repair as shown in Fig. 3b. Clockwise rotation was consistently applied to all cases while the degree of rotation and the resection path varied based on patient-specific anatomical constraints.

It is worth noting that our goal is to separate the stenotic regions from the rest of the aorta and simulate hemodynamic performance of the final reconstructed geometry. Deformation of the tissue due to clamp placement in the actual surgery was secondary to our goal. We thus simplify aorta modeling as a rigid body during the virtual planning.

The next step is to perform virtual resection of the stenotic regions by removing the vessel walls within surgeon-specified locations. Fig. 3 demonstrates two examples of resection paths using blue dash lines. The grey regions are to be removed for new graft planning. The paths to guide resection were created on the midplane of the aortic arch and started at the proximal arch, as close as possible to the clamp, and ended distal to the LSA. In Fig. 3a, the resection path in the arch was a straight line. In Fig. 3b, a straight path could not be generated due to the inclusion of the inner part of the distal AAo and the acute angle between AAo and the aortic arch. Inclusion of distal part of AAo, circled region in Fig. 3b, allowed a larger region to reconstruct the shape of the arch that could prevent the gothic arch geometry. After defining the region of repair, the lower surface was resected by performing an extruded cut through the anterior and posterior surfaces following the vessel cutting path. On the DAo side, the resection was completed by a cut perpendicular to the flow direction where the diameter of DAo started increasing distal to CoA.

## Patient-Specific Aortic Graft Design and Shape Optimization

The procedure of patient-specific graft design is shown in Fig. 4. The aim was to create a smooth arch shape starting from the distal AAo and ending at DAo that repairs both CoA and TAH. Since the CoA was resected, a tubular graft was needed to complete the DAo. In the arch region, only the lower half was removed to increase the arch diameter without affecting the supra-aortic branches. The lower arch part was connected to DAo by creating a water-slide shape in this region. Therefore, the patient-specific graft consisted of a combination of tubular and waterslide shapes.

The inner and outer curved paths needed to be defined to reconstruct and parameterize the inner and outer graft surfaces. First, the start and end points of the inner curve were determined on the edges of the resected geometry as shown in Fig. 4a. The start point $p_1$ was placed at the vertex of the

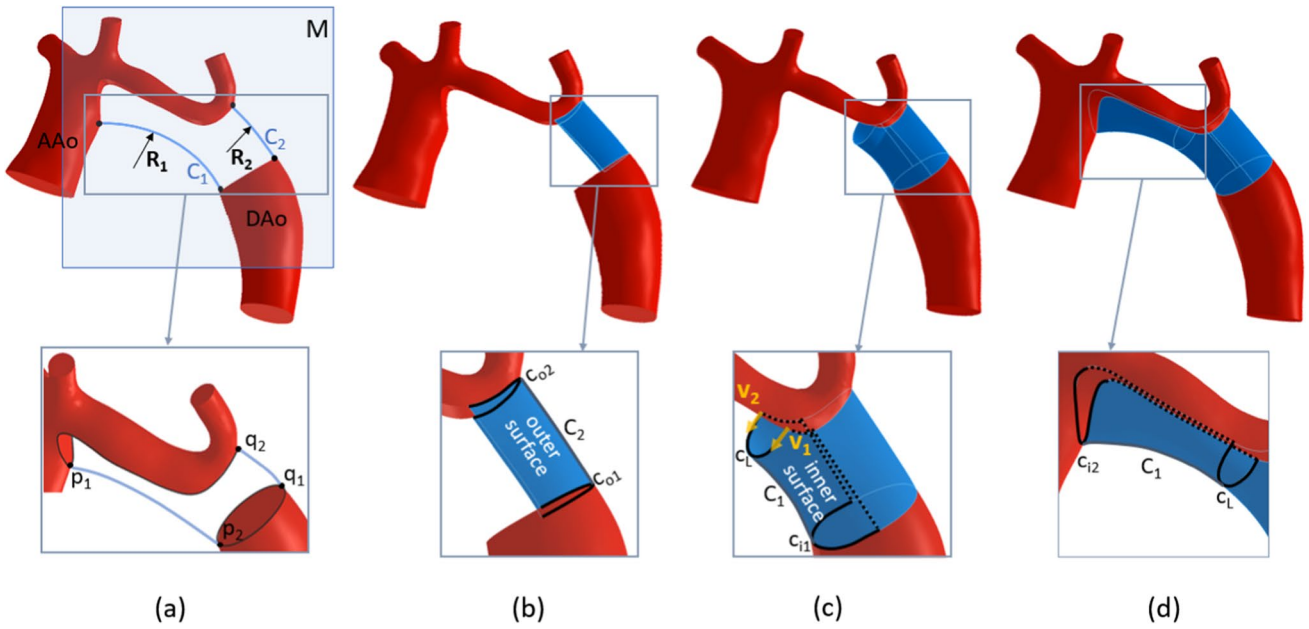


**Fig. 4** Drawings of design steps for creating novel patient specific aortic grafts for comprehensive repair: **a** creation of inner and outer guidance curves to reconstruct the surfaces of the graft **b** reconstruction of outer surface of the graft by interpolating the outer edges using the guidance curve $C_2$, **c** reconstruction of inner surface of the tubular part of the graft by interpolating the inner edges using the guidance curves, $C_1$ and the dashed curves, **d** reconstruction of the waterslide patch part of the graft by interpolating $C_L$ and $C_{i2}$ using dashed curves on the native geometry and $C_1$ as guidance curves

edge of the distal AAo, and the endpoint $p_2$ was placed at the vertex of the inner edge of the DAo, where the cut was performed. Then, the midplane M (Fig. 4a) that intersects with $p_1$, $p_2$, and axial plane of aorta were created. The inner curved path $C_1$ was created on this midplane using the points $p_1$, $p_2$, and radius $R_1$. Similarly, the outer curve with radius $R_2$ was defined on the midplane between points $q_1$ and $q_2$.

The outer surface (Fig. 4b) of the tubular part of the graft was generated by interpolating the 3D spline curves $C_{o1}$ and $C_{o2}$ using $C_2$ as the guidance curve. $C_{o1}$ and $C_{o2}$ were constructed on the outer edge of the native geometry on the DAo side and the outer edge of the native arch where the resection was performed. To reconstruct the inner surface of the tubular part of the graft, a 3D spline curve $C_L$ that completes the lower part of the circular profile in the arch was needed. The endpoints of $C_L$ were placed on the anterior and posterior edges of the native arch. A constraint was added to $C_L$ to be tangent to the inner curvature. The curve $C_L$ was created at the tangent direction ($v_1$ and $v_2$) from the surface of the native arch as shown in Fig. 4c. The curves $C_L$ and $C_{i1}$ were then interpolated using guidance curves $C_1$ and the edges of the outer graft surface (dashed lines in Fig. 4c) to reconstruct the inner surface.

Lastly, the creation of the waterslide part of the graft was performed by interpolating the curve $C_{i2}$ and $C_L$ using $C_1$ and the anterior and posterior edges (dashed lines) of the native arch as guidance curves as illustrated in Fig. 4d.

$C_{o1}$, $C_{o2}$, $C_{i1}$, $C_{i2}$, $C_{L,}$ and the 3D dashed curves on the edges of the native geometry, were formulated using B-spline S(t) in Eq. (1), where $n + 1$ is number of control points, $t$ is knot, $k$ is degree, $P_i$ is control points, and $N_{i,k}(t)$ are basis functions formulated in Eqs. (2) and (3). The spline parameters changed based on the cutting path on the native geometry.

$$S(t) = \sum_{i=0}^{n} N_{i,k}(t) P_i \tag{1}$$

$$N_{i,0}(t) = \begin{cases} 1 \text{ if } \quad t_i \le t < t_{i+1} \\ 0 \text{ otherwise} \end{cases} \tag{2}$$

$$N_{i,j}(t) = \frac{t - t_i}{t_{i+j} - t_i} N_{i,j-1}(t) + \frac{t_{i+j+1} - t}{t_{i+j+1} - t_{i+1}} N_{i+1,j-1}(t) \tag{3}$$

The optimization criteria for the shape of the graft were the lowest PSPD across the aorta and the lowest maximum TAWSS in the repaired region. The shape optimization involved two independent design parameters $R_1$ and $R_2$ to control the inner and outer curvature of the arch. The design space was determined by the maximum value of $R_1$ and minimum value of $R_2$. These values were obtained by defining the maximum, and minimum DAo and arch diameters based on the aorta anatomies and normal ranges and for

each patient [21, 22]. The CFD simulations were performed to calculate PSPD and TAWSS and until the lowest values of these parameters were obtained by varying the radii $R_1$ and $R_2$ iteratively. In the iterative process, $R_1$ was adjusted in increments of 1 mm for each case and $R_2$ was tweaked based on the midpoint between its highest and lowest values. Given that $R_2$ is relatively larger and has a minimal effect on both the aorta shape and hemodynamics we employed fewer variations.

The finalized design features a tubular graft coupled with a uniquely shaped patch, as depicted in Fig. 4. We assessed the potential for constructing this particular geometry using the electrospinning method due to its demonstrated capability to produce complex geometries, such as bifurcated grafts [23] and it's the versatility to create tissue-engineered grafts tailored to any patient size, making it a sufficient technique for our purposes. Our findings confirm the feasibility of effective manufacturing of this shape, as illustrated in Fig. 2e.

### Hemodynamics Simulations Using Non-invasively Measured Boundary Conditions

The 3D native and repaired aorta geometries were separated into volume meshes using Ansys (ANSYS, Canonsburg, PA, USA) Mesh. A mesh independence study was conducted by varying the mesh size in 0.25 mm increments, from 0.25 mm up to 1.25 mm. Using the 0.25 mm mesh size as a reference, the optimal mesh size that resulted in less than a 10% variation in both pressure drop (PD) and peak WSS was determined to be 0.5 mm. The maximum and minimum mesh sizes were set to 0.5 mm to obtain a uniform mesh and the governing Eqs. (4) and (5) below written in differential form were solved using second-order implicit scheme. In equations $\rho$ is density, $u$ is velocity, $\tau$ is stress tensor, and $t$ is time. The time step size used in the simulations was one-fifth of the acquired flow time step size from CMR data.

$$\frac{\partial \rho}{\partial t} + \nabla\left(\rho \vec{u}\right) = 0 \tag{4}$$

$$\rho \frac{D\vec{u}}{Dt} = -\nabla p + \rho \vec{g} + \nabla \tau_{ij} \tag{5}$$

The boundaries were extruded at the inlet of AAo and at the outlets [19]. The time-dependent velocity profile was acquired from CMR after applying static background correction by utilizing Qflow (Medis Medical Imaging Corporation, Leiden, the Netherlands) and was specified at the inlet. At the outlets, the Windkessel models were coupled with the CFD simulations using Ansys Fluent software. Since direct flow data at the supra-aortic branches were not available from CMR, we obtained the flow rates at the outlets of these branches based on an area-based estimation, a method that was used for previous studies due to similar constraints [24, 25]. The area-averaged flow rates were calculated by solving the governing equations and were used by Windkessel model to compute the static pressure at each boundary. The resistances in the Windkessel models were estimated patient-specifically [25] for native aortas and compliances were adapted from previous studies [26]. First, steady simulations were performed to calculate mean pressures. Then, using mean pressures ($P_{mean}$) and mean flow rates ($Q_{mean}$), the patient specific resistances were obtained. Lastly, time-dependent simulations were performed using Windkessel boundary conditions. The CFD procedure was summarized in Fig. 5. The patient-specific resistances at each outlet of native aortas were found using the equations shown in Fig. 5b and remained unchanged for the repaired aortas.

In Fig. 5b, i represents each outlet, P is pressure, $R_p$ is peripheral resistance, $R_d$ is distal resistance, and C is compliance. In the simulations, blood viscosity and density were assumed to be $3.71 \times 10^{-3}$ kg/(m s) and 1060 kg/m$^3$, respectively. The simulations were performed using the k-epsilon turbulence model for 10 cardiac cycles and the converged results were analyzed.

## Results

### Study Design

In this study, six patients ($n = 6$) were included who were diagnosed with both CoA and TAH. The patient demographics are provided in Table 1. The TAH diagnosis was defined by the patient's transverse arch diameter being below the normal range. The normal range differed based on patient's BSA, therefore, for cases 3, 4, and 5, the normal range and z-scores were calculated based on [21] and for cases 1, 2, and 6 they were calculated based on [22]. Negative z-score was an indication of how many standard deviations below is the TAH from the average of the normal range. The data was acquired as part of an Institutional Review Board (IRB) approved retrospective study.

Virtual surgical planning was performed in patients to repair CoA and TAH simultaneously by increasing the cross-sectional areas of narrowed regions. Furthermore, aorta shape was optimized to achieve desirable hemodynamics. TAH diameters fell into normal range for each patient after the comprehensive repair. The final optimal values of $R_1$ and $R_2$ and the curve lengths were listed in Table 2. On average, eight iterations were performed per case.

Narrowed regions of the aorta cause increased systolic pressure drop (PSPD) and increased maximum time-averaged wall shear stress (TAWSS). PSPD that is higher than 20 mmHg is an indicator for intervention [6] for aortic

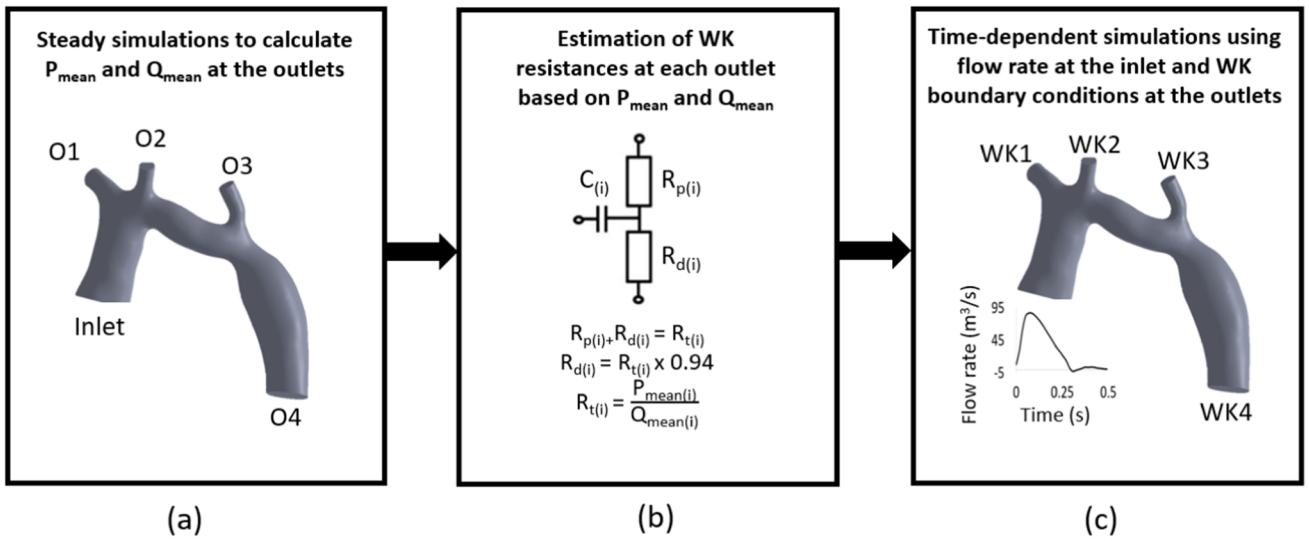


**Fig. 5** Patient-specific simulations in three steps: **a** steady simulations using non-invasively measured data, **b** estimation of Windkessel parameters from steady simulation results, and **c** time-dependent simulations coupled with Windkessel boundary conditions at the outlets

**Table 1** Patient demographics

| | BSA | Age | Cardiac output (L/min) | TAH diameter (mm) | Normal range (mm) | z-score | CoA diameter (mm) |
|---|---|---|---|---|---|---|---|
| Case 1 | 1.27 | 9 y | 5.62 | 12.10 | 13.39–18.52 | − 2.64 | 7.84 |
| Case 2 | 0.9 | 8 y | 3.85 | 9.34 | 10.42–15.56 | − 2.66 | 8.36 |
| Case 3 | 0.38 | 9 mo | 1.83 | 5.58 | 6.10–10.69 | − 2.04 | 5.13 |
| Case 4 | 0.44 | 10 mo | 1.41 | 6.18 | 6.63–11.63 | − 1.99 | 4.05 |
| Case 5 | 0.54 | 2 y | 2.20 | 5.88 | 7.28–12.77 | − 2.23 | 6.59 |
| Case 6 | 1.88 | 15 y | 8.81 | 14.32 | 17.41–22.54 | − 4.1 | 12.44 |

The negative *z* scores indicate the TAH diameter is below the normal range

**Table 2** Optimal values of $R_1$ and $R_2$ and the resulting curve lengths $C_1$ and $C_2$

| | Optimal $R_1$ (mm) | Curve ($C_1$) length (mm) | Optimal $R_2$ (mm) | Curve ($C_2$) length (mm) |
|---|---|---|---|---|
| Case 1 | 9 | 20.8 | 85 | 10.26 |
| Case 2 | 15 | 23.5 | 59 | 13.7 |
| Case 3 | 18 | 21.0 | 59 | 9.9 |
| Case 4 | 12 | 24.8 | 35 | 12.6 |
| Case 5 | 7 | 11.7 | 24 | 8.2 |
| Case 6 | 17 | 41.0 | 390 | 27.6 |

defects. Furthermore, the TAWSS is associated with rupture, aneurysm formation, and platelet activation [27]. Previous studies suggested that high TAWSS (15–45 Pa) is related to thrombosis [28].Therefore, we focused primarily on minimizing PSPD and TAWSS when optimizing the patient-specific grafts. While we did not factor in low WSS in our optimization framework, we investigated the minimum TAWSS and instantaneous WSS during the diastolic phase. The lowest WSS observed in the repaired cases was 0.41 Pa, significantly higher than the 0.1 Pa threshold that is linked to thrombosis [29].

Moreover, we considered the flow velocity and vorticity in our comparison of the different repairs, as WSS is intrinsically tied to changes in flow fields, and each repair method may produce unique flow characteristics. Lastly, we reported oscillatory shear index (OSI) in this section to (1) ascertain that post-repair OSI values align with standard values from existing literature, and (2) present it alongside TAWSS. This is crucial since high OSI combined with low TAWSS values can potentially contribute to tissue damage [30].

## PSPD

The PSPD between AAo and DAo, and the maximum TAWSS in the repaired region were obtained from the initial comprehensive repairs 1 and 2, that were performed after the virtual resections shown in Fig. 3a and b, respectively.

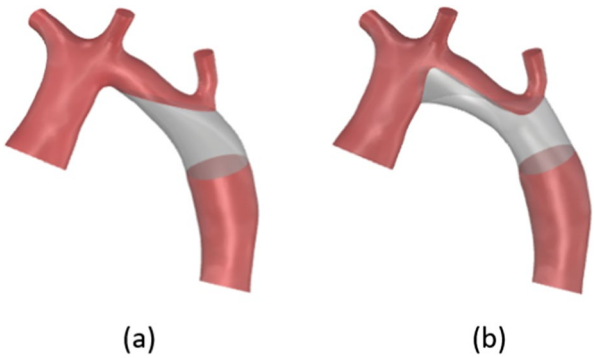


**Fig. 6** Anatomies after comprehensive repairs 1 **a** and 2 **b**. A smoother transition from AAo to arch is observed in **b**

**Table 3** PSPD and maximum TAWSS results of comprehensive repair 1 and comprehensive repair 2

| | PSPD (mmHg) | | Maximum TAWSS (Pa) | |
|---|---|---|---|---|
| | Comprehensive repair 1 | Comprehensive repair 2 | Comprehensive repair 1 | Comprehensive repair 2 |
| Case 1 | 10.21 | 9.27 | 7.2 | 6.5 |
| Case 2 | 16.50 | 14.6 | 14.7 | 10.1 |
| Case 3 | 24.51 | 16.86 | 47.5 | 28.2 |
| Case 4 | 6.12 | 5.33 | 10.5 | 7.1 |
| Case 5 | 24.81 | 15.73 | 27.2 | 18.3 |
| Case 6 | 12.22 | 11.08 | 24.5 | 16.7 |

The resulting anatomies and hemodynamics are compared in Fig. 6 and Table 3, respectively. For all the cases, the repair 2 showed better hemodynamics than repair 1 due to the extended design region and smoother flow path from AAo to DAo. Therefore, only comprehensive repair 2 was optimized and its results were compared against the native geometries in the remainder of the paper.

To compare the performance of the comprehensive repair against a less invasive isolated CoA repair, we performed patient-specific CoA repairs using virtual stents. The virtual stents were selected from commercially available stents [31] based on DAo diameter of each patient. The CoA repair was done by replacing stenotic region with a tubular loft until the diameter of narrowed region reached DAo diameter [19].

The pressure distributions at peak systole were shown and virtual repairs were compared against native geometries in Fig. 7. The PSPD between AAo and DAo were provided in Table 4. The isolated CoA repair was unable to reduce the PSPD below 20 mmHg for case 3 and case 5. For case 2, the improvement in PSPD was insignificant. After the repair of CoA using a virtual stent, high pressure in AAo was persistent in case 3 and case 5. The sharp change in flow direction from AAo to arch in case 3 and narrow region proximal to the arch in case 5 were responsible for high pressure in AAo. Virtual comprehensive repair of CoA and TAH using a patient-specific novel graft decreased the pressure in AAo and improved PSPD significantly for these two cases.

The percent PSPD improvements after the CoA repair and the comprehensive repair were plotted in Fig. 8a and b, respectively. To determine the relationship between arch dimensions and results, a diameter ratio of CoA and TAH was calculated (the higher the ratio, the greater geometrical significance of the TAH). A linear correlation with $R^2 = 0.84$ (by Pearson) was observed between percent PSPD improvement after CoA repair and the diameter ratio of CoA and

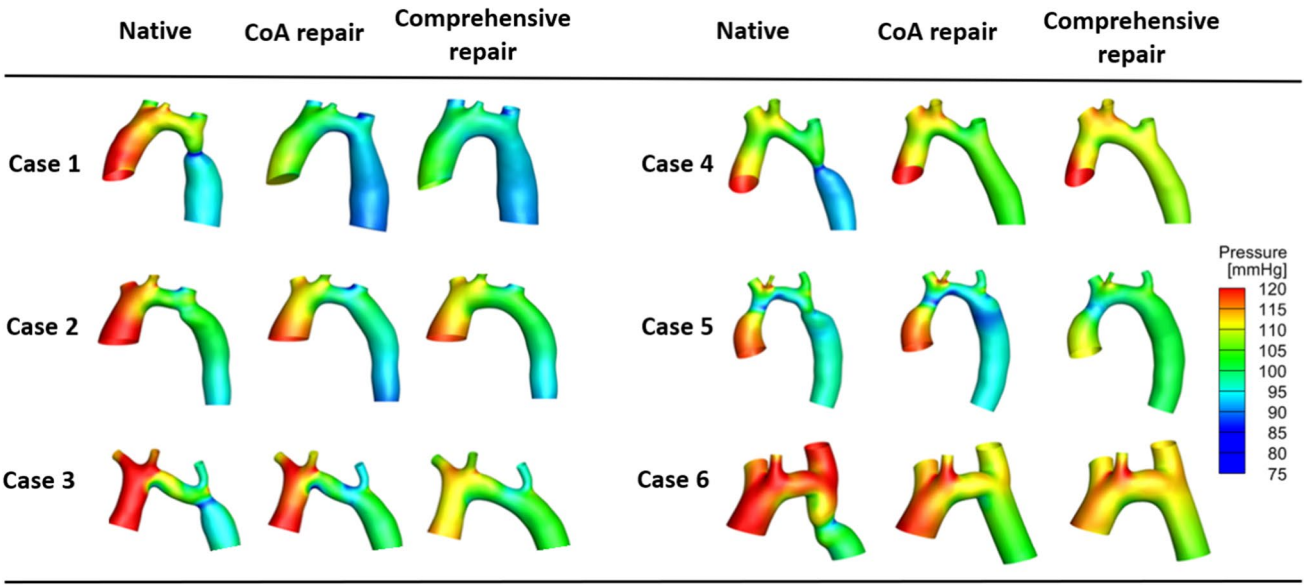


**Fig. 7** The pressure distributions normal to the surface of the aorta walls

**Table 4** PSPD [mmHg] measured between AAo and DAo

| | Native | CoA repair | Comprehensive repair |
|---|---|---|---|
| Case 1 | 24.72 | 15.42 | 9.27 |
| Case 2 | 17.45 | 17.26 | 14.60 |
| Case 3 | 44.62 | 30.94 | 16.86 |
| Case 4 | 11.21 | 6.19 | 5.33 |
| Case 5 | 35.36 | 36.60 | 15.73 |
| Case 6 | 24.78 | 18.17 | 11.08 |

TAH (Fig. 8a). The higher the ratio of CoA diameter to TAH diameter, the lower the improvement in PSPD was after the CoA repair. Furthermore, the PSPD was generally improved significantly (more than 40% for four out of six cases) after the comprehensive repair in cases that showed small PSPD improvement after the CoA repair. For example, PSPD in case 5 showed no significant difference after the CoA repair, however, was decreased by 77% with the comprehensive repair. Case 5 was the only patient aorta that had a smaller diameter of TAH than the diameter of CoA. Although the CoA was repaired using a virtual stent and the diameter in the narrow region of DAo was increased, there were still major restrictions to blood flow in the arch and distal AAo, which caused high PSPD overall in case 5. No significant correlation was observed between percent PSPD improvement after comprehensive repair and the ratio of CoA diameter to TAH diameter (Fig. 8b).

## TAWSS

Similarly, the TAWSS results were shown in Fig. 9 and the maximum values of TAWSS in the repaired region were provided for each case in Table 5. A reduced TAWSS was observed after the repairs. However, it remained relatively high after the CoA repair, especially in cases with a lower ratio of CoA diameter to TAH diameter. The comprehensive repair showed further improvement in maximum values of TAWSS in all cases compared to the isolated CoA repair.

Although the isolated CoA repair reduced the PSPD sufficiently for four out of six cases, the maximum TAWSS remained higher than 15 Pa for five of the six cases. The comprehensive repair successfully reduced the maximum TAWSS in the arch and DAo. However, they remained higher than 15 Pa for case 3 and case 5 (28.2 and 18.3 Pa, respectively) even after the comprehensive repair. As established in previous research [28], this threshold is the minimal value at which thrombosis can initiate.

Although the minimum values of TAWSS was not considered when optimizing the aorta geometries, we verified that in the repaired areas, the minimum TAWSS values were much higher (as seen in Fig. 9) than 0.4 Pa, the lower threshold that is associated with atherosclerosis [28].

## Oscillatory Shear Index

Oscillatory shear index (OSI) is another important parameter that represents the change of direction of the WSS vector. OSI is deleterious when it is observed with low WSS. OSI in native and repaired geometries were investigated in DAo and the results were provided in Table 6 with the TAWSS and OSI averaged over the DAo walls. We observed that in the repaired geometries, the OSI results were closer to the normal values [32]. Although OSI was not always reduced after the comprehensive repair, since our cases have relatively high WSS, the risks of tissue damage are low.

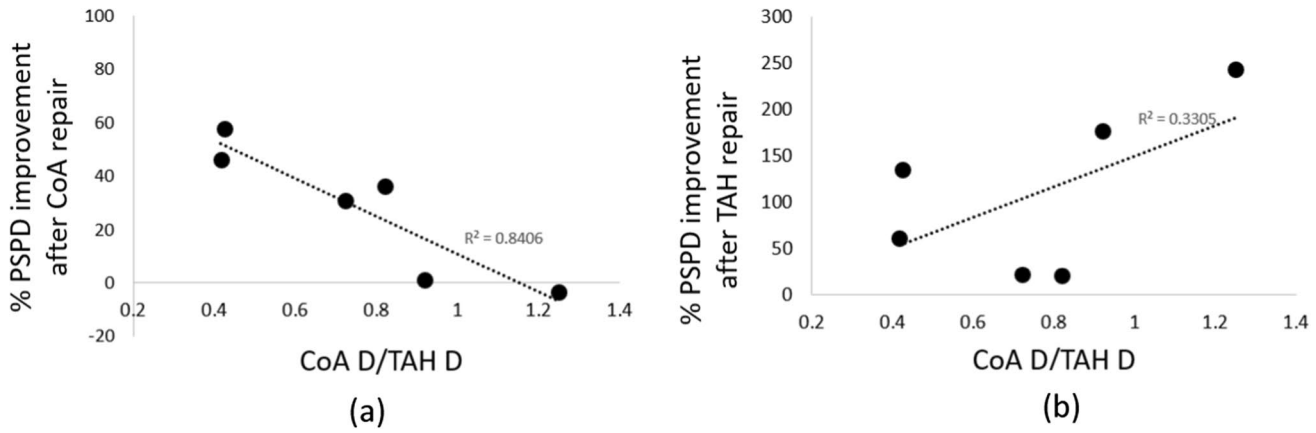


**Fig. 8** Percent PSPD improvement after **a** CoA repair, and **b** comprehensive repair. The x-axes indicate the ratio of the diameter of CoA to the diameter of TAH in native geometries

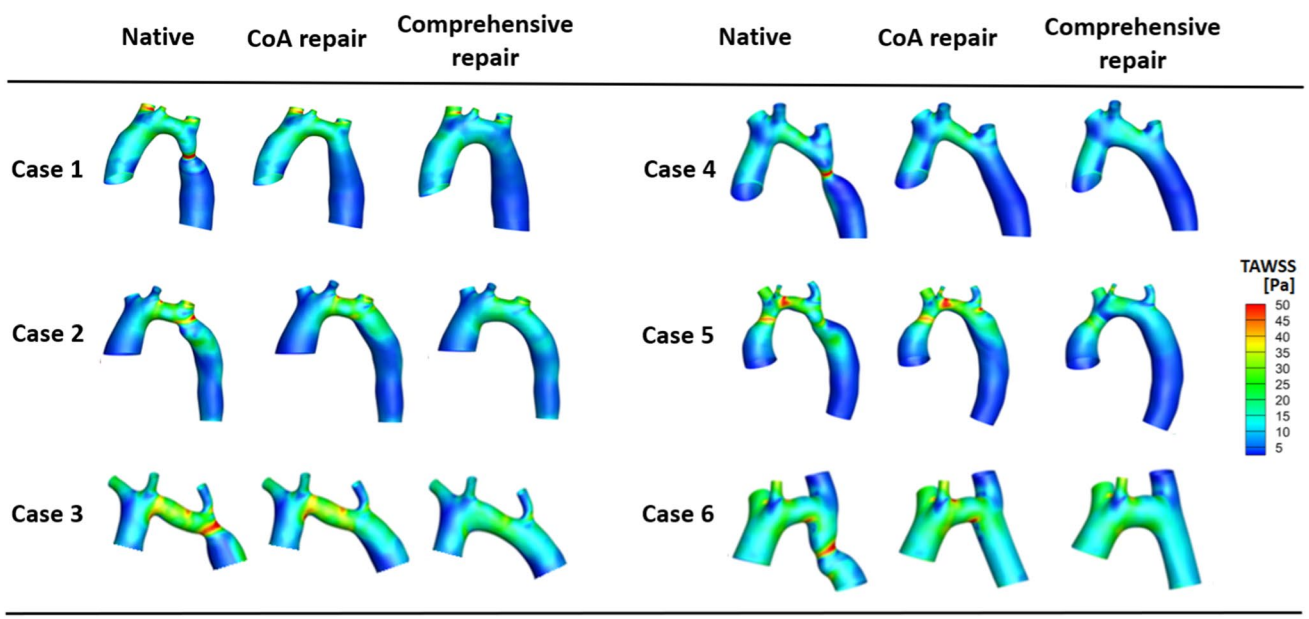


**Fig. 9** The TAWSS distributions on the aorta walls

**Table 5** Maximum values of TAWSS [Pa] on the walls of repaired region

| | Native | CoA repair | Comprehensive repair |
|---|---|---|---|
| Case 1 | 38 | 18 | 6 |
| Case 2 | 26 | 16 | 10 |
| Case 3 | 70 | 34 | 28 |
| Case 4 | 18 | 10 | 7 |
| Case 5 | 50 | 27 | 18 |
| Case 6 | 38 | 21 | 11 |

## Velocity and Vorticity Magnitude

Lastly, we investigated the maximum velocities and vorticity magnitude in the native and virtually repaired cases. The comparison of two virtual repairs showed that the high velocities in the aortic arch were further decreased after the comprehensive repair. The average percent decrease in velocity and vorticity magnitude at peak systole were $30 \pm 5\%$ and $15 \pm 7\%$ after the CoA repair, and $19 \pm 13\%$ and $25 \pm 6\%$ after the comprehensive repair, respectively.

Decrease in velocity and vorticity magnitude were previously shown in virtually repaired CoA [33]. Our findings support that. Furthermore, repairing the TAH with CoA prevents the jet flow from arch to DAo that causes the flow to hit the proximal DAo walls and create secondary flow patterns as shown in Fig. 10.

## Discussion

In this study, two different patient-specific virtual repairs were performed for six cases with comorbid CoA and TAH. The hemodynamic changes were investigated to compare

**Table 6** TAWSS and OSI averaged over DAo surface

| | TAWSS [Pa] | | | OSI | | |
|---|---|---|---|---|---|---|
| | Native | CoA repair | Comprehensive repair | Native | CoA repair | Comprehensive repair |
| Case 1 | 5.25 | 2.62 | 1.95 | 0.35 | 0.41 | 0.41 |
| Case 2 | 4.25 | 2.71 | 2.23 | 0.09 | 0.09 | 0.08 |
| Case 3 | 18.24 | 13.88 | 10.89 | 0.03 | 0.03 | 0.04 |
| Case 4 | 4.23 | 1.95 | 1.82 | 0.01 | 0.01 | 0.01 |
| Case 5 | 5.75 | 5.43 | 3.74 | 0.08 | 0.09 | 0.12 |
| Case 6 | 14.96 | 8.94 | 7.28 | 0.12 | 0.15 | 0.14 |

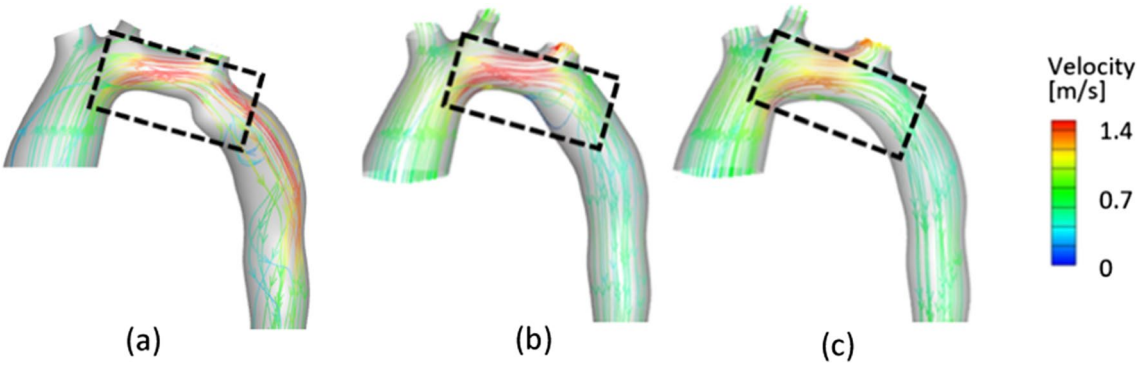


**Fig. 10** Velocity streamlines **a** in the native aorta, **b** after CoA repair, and **c** after comprehensive repair. The magnitude of velocity and vorticity in the arch further decreased after comprehensive repair

the performance of isolated CoA repair and comprehensive repair of both CoA and TAH. Comprehensive repair showed further improvements in both PSPD and TAWSS results. The virtual repair of CoA alone was insufficient to reduce the PSPD below 20 mmHg in two (cases 3 and 5) out of six cases. However, the PSPDs of native models of these cases were already high. As seen in Fig. 7, the native geometries of case 3 and case 5 have smaller TAH diameters compared to the diameters of AAo and DAo, and since the CoA repair does not alter the TAH diameter, the PSPDs remained high in these cases. Considering the flow rates and pressure boundary conditions applied to these cases, reducing the PSPD further was challenging. Notably, a PSPD value of 20 mmHg is often considered as the threshold indicating the need for intervention. By this standard, our comprehensive repair effectively reduced the PSPD to below 20 mmHg in these severe cases. On the other hand, case 4 exhibited a lower PSPD in its native anatomy despite the presence of a severe CoA. The flow percentage to the DAo was also notably greater than in other cases in this study. While we lack data on collateral formation from patient records, this decreased PSPD and increased inflow to the DAo might suggest the development of collaterals. Nevertheless, these observations do not diminish the main aim of our study, which is to compare two different repairs. In this regard, our comparative analysis maintains its relevance and significance.

The results of TAWSS and OSI from the repaired geometries were compared against the values that were measured from healthy subjects in previous studies [34, 35]. However, in the literature, the TAWSS and OSI in aortas of healthy subjects were obtained from MRI data. The discrepancy between MRI measured and CFD calculated wall parameters is known [36]. When the mesh is sufficiently small, CFD calculated WSS is generally higher than MRI measured WSS [36] and our results show a similar trend. In contrast, since the OSI is a dimensionless parameter, the values were in the same range as the ones that were measured via the MRI from the normal aortas. Additionally, the normal values of WSS differ in patients of different ages [36]. High WSS in the aorta is associated with the initiation of aneurysm formation [37], atherosclerotic plaque destabilization, and rupture [38]. While the isolated CoA repair effectively reduced elevated WSS levels in the DAo, a more pronounced decrease in remaining high WSS values in the aortic arch was observed following the comprehensive repair across all cases.

An inversed linear correlation between percent PSPD improvement and diameter ratio of CoA to TAH was observed after our analysis. The diameter ratio reflects the geometrical significance of TAH, therefore, treating the TAH would likely improve PSPD further. This study raises the finding that it may be important to study the relationship of diameter ratio to PSPD improvement as part of clinical study.

One limitation of the current study is the assumption of rigid walls for CFD simulations. Aorta walls show viscoelastic behavior, and the movement of the walls affects the wall parameters [39]. However, in this study, our primary goal was to provide the comparison of two different repairs for which we used the exact same numerical approach. The use of rigid walls, though not perfectly mimicking real-world conditions, is a simplification to help create a standardized framework that underscores the differences between the two repair techniques in our study. The implications of aorta wall's viscoelastic properties can be explored in a future study to provide a more comprehensive understanding of the hemodynamics post-repair. Additionally, only six cases were included in this study due to a lack of patient data. However, the anatomies of the aortas of the patients were distinctive, which helped in observing different improvements after two different repairs. Unfortunately, post-operative data from the patients involved in our study was not available for validating our virtual repairs. In subsequent research, it would be beneficial to compare these findings

with real surgical outcomes to evaluate the reliability and precision of our results.

The standard of care to repair CoA involves placing surgical clamps in the aorta to resect the CoA and perform end-to-end anastomosis, whereas TAH repair is typically performed under cardiopulmonary bypass by reconstructing the hypoplastic arch with a patch. The simple CoA repair using clamps provides good early and long-term results, but the clamp placed in the aortic arch may not allow access to the arch to repair a possible TAH. In this study, we propose an alternative approach that includes clamp placement in the proximal arch to perform both CoA and TAH repairs that avoid the bypass. The placement of the clamp allows defining the boundaries of regions that require repair and how far we could extend the repair in the aortic arch. One limitation of this approach is that it may result in longer suture lines in the aortic arch if the hypoplasia exists in the proximal arch or AAo. A longer suture line requires a longer repair time that increases the risk of neurological injuries [40]. Surgeons may prefer to perform repair under bypass. However, the cases studied in this paper were not diagnosed with AAo hypoplasia or proximal arch hypoplasia. While our modeling primarily emphasizes the repair of CoA and TAH, it has the potential to be extended to several aortic repair procedures that require graft or patch placements. For instance, our approach can be adapted to develop a patient-specific tubular graft for aortic aneurysm repair [41]. Alternatively, it could be used to design a waterslide-shaped patch segment for enhancing the aortic arch [42]. In this study, our purpose was to demonstrate the benefit and possibility of repairing TAH by using aortic clamps. Hence, we showed the feasibility of comprehensive repair by designing a tissue-engineered graft that will be manufactured before the surgery. We aim to reduce surgery time by providing pre-operative repair plans and the final optimized geometry for patient-specific 3D printed grafts, which could further improve the feasibility of TAH repair by using aortic clamps.

## Conclusion

We investigated hemodynamic improvements after repairing isolated CoA using a virtual stent and repairing CoA and TAH simultaneously using a graft that has a novel shape of a combination of a tubular shape and a waterslide vascular patch. We showed that the minimally invasive CoA repair alone was not always sufficient to reduce the PSPD and may not be the best repair for every patient. Furthermore, comprehensive repair involved a larger part of the aorta allowing engineers to design a better shape with improved hemodynamics. We showed that patient-specific virtual planning for aortic repairs could play a significant role in clinical decision making. Predicting the hemodynamic outcomes of different repairs using CFD before the surgery provides information that could help doctors when selecting the optimal repair technique on a patient-specific basis.

**Acknowledgments** This research was supported by the National Institutes of Health (award #R01HL143468 and #R21HD090671), and the Maryland Technology Development Corporation (Maryland Innovation Initiative Award # 1120-004). This research project was conducted using computational resources at the Advanced Research Computing at Hopkins (ARCH) (https://www.arch.jhu.edu).

**Funding** Funding was provided by NIH (R01HL143468, R33HD090671, R21HD090671).

## Declarations

**Conflict of interest** Axel Krieger and Xiaolong Liu are founders of and hold shares of stock options in CorFix Medical, Inc. The results of the study discussed in this publication could affect the value of CorFix Medical Inc. This arrangement has been reviewed and approved by the Johns Hopkins University in accordance with its conflict-of-interest policies. Jed Johnson is a co-founder and stockholder of Nanofiber Solutions.

## References

1. Alkashkari, W., S. Albugami, and Z. M. Hijazi. Management of coarctation of the aorta in adult patients: state of the art. *Korean Circ. J.* 49:298–313, 2019. https://doi.org/10.4070/kcj.2018.0433.
2. Meadows, J., M. Minahan, D. B. McElhinney, et al. Intermediate outcomes in the prospective, multicenter coarctation of the aorta stent trial (COAST). *Circulation*. 131:1656–1664, 2015. https://doi.org/10.1161/CIRCULATIONAHA.114.013937.
3. Yang, L., X. Chua, D. D. Rajgor, et al. A systematic review and meta-analysis of outcomes of transcatheter stent implantation for the primary treatment of native coarctation. *Int. J. Cardiol.* 223:1025–1034, 2016. https://doi.org/10.1016/j.ijcard.2016.08.295.
4. LaDisa, J. F., R. J. Dholakia, C. A. Figueroa, et al. Computational simulations demonstrate altered wall shear stress in aortic coarctation patients treated by resection with end-to-end anastomosis. *Congenit. Heart. Dis.* 6:432–443, 2011. https://doi.org/10.1111/j.1747-0803.2011.00553.x.
5. Wendell, D. C., I. Friehs, M. M. Samyn, et al. Treating a 20 mmHg gradient alleviates myocardial hypertrophy in experimental aortic coarctation. *J. Surg. Res.* 218:194–201, 2017. https://doi.org/10.1016/j.jss.2017.05.053.
6. Nguyen, L., and S. C. Cook. Coarctation of the aorta: strategies for improving outcomes. *Cardiol. Clin.* 33:521–530, 2015. https://doi.org/10.1016/j.ccl.2015.07.011.
7. Ma, Z.-L., J. Yan, S.-J. Li, et al. Coarctation of the aorta with aortic arch hypoplasia: midterm outcomes of aortic arch reconstruction with autologous pulmonary artery patch. *Chin. Med. J. (Engl.)*. 130:2802–2807, 2017. https://doi.org/10.4103/0366-6999.215279.
8. Thomson, J., A. Mulpur, R. Guerrero, et al. Outcome after extended arch repair for aortic coarctation. *Heart*. 2006. https://doi.org/10.1136/hrt.2004.058685.
9. Soynov, I., Y. Sinelnikov, Y. Gorbatykh, et al. Modified reverse aortoplasty versus extended anastomosis in patients with coarctation of the aorta and distal arch hypoplasia. *Eur. J. Cardio-Thorac. Surg.* 53:254–261, 2018. https://doi.org/10.1093/ejcts/ezx249.

10. Wen, S., J. Cen, J. Chen, et al. The application of autologous pulmonary artery in surgical correction of complicated aortic arch anomaly. *J. Thorac. Dis.* 8:3301–3306, 2016.
11. Quennelle, S., A. J. Powell, T. Geva, and A. Prakash. Persistent aortic arch hypoplasia after coarctation treatment is associated with late systemic hypertension. *J. Am. Heart Assoc. Cardiovasc. Cerebrovasc. Dis.*4:e001978, 2015. https://doi.org/10.1161/JAHA.115.001978.
12. Rakhra, S. S., M. Lee, A. J. Iyengar, et al. Poor outcomes after surgery for coarctation repair with hypoplastic arch warrants more extensive initial surgery and close long-term follow-up. *Interact. Cardiovasc. Thorac. Surg.* 16:31–36, 2013. https://doi.org/10.1093/icvts/ivs301.
13. Liu, X., N. Hibino, Y.-H. Loke, et al. Surgical planning and optimization of patient-specific Fontan grafts with uncertain postoperative boundary conditions and anastomosis displacement. *IEEE Trans. Biomed. Eng.* 2022. https://doi.org/10.1109/TBME.2022.3170922.
14. Loke, Y.-H., B. Kim, P. Mass, et al. Role of surgeon intuition and computer-aided design in Fontan optimization: a computational fluid dynamics simulation study. *J. Thorac. Cardiovasc. Surg.* 160:203-212.e2, 2020. https://doi.org/10.1016/j.jtcvs.2019.12.068.
15. Trusty, P. M., Z. A. Wei, T. C. Slesnick, et al. The first cohort of prospective Fontan surgical planning patients with follow up data: how accurate is surgical planning? *J. Thorac. Cardiovasc. Surg.* 157:1146–1155, 2019. https://doi.org/10.1016/j.jtcvs.2018.11.102.
16. Wu, Q., V. Cleveland, S. Aslan, et al. Hemodynamics of convergent cavopulmonary connection with ventricular assist device for Fontan surgery: a computational and experimental study. In: Bioinformatics, 2023
17. Liu, X., B. Kim, Y.-H. Loke, et al. Semi-automatic planning and three-dimensional electrospinning of patient-specific grafts for Fontan surgery. *IEEE Trans. Biomed. Eng.* 69:186–198, 2022. https://doi.org/10.1109/TBME.2021.3091113.
18. Armstrong, A. K., J. D. Zampi, L. M. Itu, and L. N. Benson. Use of 3D rotational angiography to perform computational fluid dynamics and virtual interventions in aortic coarctation. *Catheter. Cardiovasc. Interv.* 95:294–299, 2020. https://doi.org/10.1002/ccd.28507.
19. Aslan, S., X. Liu, Q. Wu, et al. Virtual planning and simulation of coarctation repair in hypoplastic aortic arches: is fixing the coarctation alone enough? In: Bioinformatics, pp. 138–143, 2022
20. Backer, C. L., C. Mavroudis, E. A. Zias, et al. Repair of coarctation with resection and extended end-to-end anastomosis. *Ann. Thorac. Surg.* 66:1365–1370, 1998. https://doi.org/10.1016/S0003-4975(98)00671-7.
21. Lopez, L., S. Colan, M. Stylianou, et al. Relationship of echocardiographic z scores adjusted for body surface area to age, sex, race, and ethnicity: the pediatric heart network normal echocardiogram database. *Circ. Cardiovasc. Imaging.* 10:e006979, 2017. https://doi.org/10.1161/CIRCIMAGING.117.006979.
22. Kaiser, T., C. J. Kellenberger, M. Albisetti, et al. Normal values for aortic diameters in children and adolescents—assessment in vivo by contrast-enhanced CMR-angiography. *J. Cardiovasc. Magn. Reson.* 10:56, 2008. https://doi.org/10.1186/1532-429X-10-56.
23. Aslan, S., Y.-H. Loke, P. Mass, et al. Design and simulation of patient-specific tissue-engineered bifurcated right ventricle-pulmonary artery grafts using computational fluid dynamics. In: 2019 IEEE 19th International Conference on Bioinformatics and Bioengineering (BIBE). pp. 1012–1018, 2019
24. Itu, L., D. Neumann, V. Mihalef, et al. Non-invasive assessment of patient-specific aortic haemodynamics from four-dimensional flow MRI data. *Interface Focus.* 8:20170006, 2017. https://doi.org/10.1098/rsfs.2017.0006.
25. Aslan, S., P. Mass, Y.-H. Loke, et al. Non-invasive prediction of peak systolic pressure drop across coarctation of aorta using computational fluid dynamics. *Annu. Int. Conf. IEEE Eng. Med. Biol. Soc.* 2020:2295–2298, 2020. https://doi.org/10.1109/EMBC44109.2020.9176461.
26. Karmonik, C., A. Brown, K. Debus, et al. CFD challenge: predicting patient-specific hemodynamics at rest and stress through an aortic coarctation. In: Statistical atlases and computational models of the heart. Imaging and modelling challenges, edited by O. Camara, T. Mansi, M. Pop, et al. Berlin: Springer, 2014, pp. 94–101.
27. Dux-Santoy, L., A. Guala, J. Sotelo, et al. Low and oscillatory wall shear stress is not related to aortic dilation in patients with bicuspid aortic valve. *Arterioscler. Thromb. Vasc. Biol.* 40:e10–e20, 2020. https://doi.org/10.1161/ATVBAHA.119.313636.
28. Boumpouli, M., E. L. Sauvage, C. Capelli, et al. Characterization of flow dynamics in the pulmonary bifurcation of patients with repaired tetralogy of fallot: a computational approach. *Front. Cardiovasc. Med.* 8:703717, 2021.
29. Hathcock, J. J. Flow effects on coagulation and thrombosis. *Arterioscler. Thromb. Vasc. Biol.* 26:1729–1737, 2006. https://doi.org/10.1161/01.ATV.0000229658.76797.30.
30. Wang, H., D. Balzani, V. Vedula, et al. On the potential self-amplification of aneurysms due to tissue degradation and blood flow revealed from FSI simulations. *Front. Physiol.*12:785780, 2021. https://doi.org/10.3389/fphys.2021.785780.
31. Peters, B., P. Ewert, and F. Berger. The role of stents in the treatment of congenital heart disease: current status and future perspectives. *Ann. Pediatr. Cardiol.* 2:3–23, 2009. https://doi.org/10.4103/0974-2069.52802.
32. Bürk, J., P. Blanke, Z. Stankovic, et al. Evaluation of 3D blood flow patterns and wall shear stress in the normal and dilated thoracic aorta using flow-sensitive 4D CMR. *J. Cardiovasc. Magn. Reson.* 14:84, 2012. https://doi.org/10.1186/1532-429X-14-84.
33. Rafieianzab, D., M. A. Abazari, M. Soltani, and M. Alimohammadi. The effect of coarctation degrees on wall shear stress indices. *Sci. Rep.* 11:12757, 2021. https://doi.org/10.1038/s41598-021-92104-3.
34. Kwon, S., J. Feinstein, R. Dholakia, and J. LaDisa. Quantification of local hemodynamic alterations caused by virtual implantation of three commercially available stents for the treatment of aortic coarctation. *Pediatr. Cardiol.* 2013. https://doi.org/10.1007/s00246-013-0845-7.
35. Callaghan, F. M., and S. M. Grieve. Normal patterns of thoracic aortic wall shear stress measured using four-dimensional flow MRI in a large population. *Am. J. Physiol. Heart Circ. Physiol.* 315:H1174–H1181, 2018. https://doi.org/10.1152/ajpheart.00017.2018.
36. Miyazaki, S., K. Itatani, T. Furusawa, et al. Validation of numerical simulation methods in aortic arch using 4D Flow MRI. *Heart Vessels.* 32:1032–1044, 2017. https://doi.org/10.1007/s00380-017-0979-2.
37. Arzani, A., and S. C. Shadden. Characterizations and correlations of wall shear stress in aneurysmal flow. *J. Biomech. Eng.* 2016. https://doi.org/10.1115/1.4032056.
38. Dolan, J. M., J. Kolega, and H. Meng. High wall shear stress and spatial gradients in vascular pathology: a review. *Ann. Biomed. Eng.* 41:1411–1427, 2013. https://doi.org/10.1007/s10439-012-0695-0.
39. Lopes, D., H. Puga, J. C. Teixeira, and S. F. Teixeira. Influence of arterial mechanical properties on carotid blood flow: comparison of CFD and FSI studies. *Int. J. Mech. Sci.* 160:209–218, 2019. https://doi.org/10.1016/j.ijmecsci.2019.06.029.
40. Beckmann, E., and A. S. Jassar. Coarctation repair—redo challenges in the adults: what to do? *J. Vis. Surg.* 4:76, 2018. https://doi.org/10.21037/jovs.2018.04.07.

41. Hong, J. C., J. S. Coselli, and O. Preventza. The dos and don'ts of open and endovascular thoracoabdominal aortic aneurysm repair. *Innovations*. 15:513–520, 2020. https://doi.org/10.1177/1556984520967304.
42. Uzzaman, M. M., N. E. Khan, B. Davies, et al. Long-term outcome of interrupted arch repair with direct anastomosis and homograft augmentation patch. *Ann. Thorac. Surg*. 105:1819–1826, 2018. https://doi.org/10.1016/j.athoracsur.2018.01.035.